Medium-energy ion scattering investigation of the surface and subsurface structure of three-dimensional $HoSi_{2-x}$ grown on Si(111)

T. J. Wood,[1] C. Bonet,[1] T. C. Q. Noakes,[2] P. Bailey,[2] and S. P. Tear[1,*]
[1]*Department of Physics, University of York, Heslington, York, YO10 5DD, United Kingdom*
[2]*CCLRC Daresbury Laboratory, Daresbury, Warrington, WA4 4AD, United Kingdom*
(Received 23 January 2006; revised manuscript received 13 March 2006; published 8 June 2006)

The surface structure of the three-dimensional (3D) holmium silicide grown on Si(111) has been determined using medium-energy ion scattering. Using this technique, it has been possible for the first time to elucidate the structure of the surface bilayer, free from complications due to lower layer atoms. It has been established that this surface generally displays sixfold symmetry which has been attributed to a mixture of reversed and nonreversed buckled bilayers (*B*-type and *A*-type respectively). A threefold surface has also been observed which is due to the preferential growth of an *A*-type buckled bilayer. It is proposed that the underlying vacancy network is the cause of the mixed phase on the surface. Both phases show consistent lattice spacings with the surface Si bilayer in the *A*/*B* mixed phase sitting 1.97 ± 0.01 Å above the first Ho layer, with a vertical buckling separation of 0.79 ± 0.04 Å. Such terminations are present on top of the established layered structure of the 3D silicide, with a Ho-Ho vertical spacing of 4.01 ± 0.02 Å, which is compressed relative to the bulk value due to the relief of strain at the interface.

DOI: 10.1103/PhysRevB.73.235405 PACS number(s): 68.55.−a, 68.65.−k, 68.35.Ct, 68.49.Sf

I. INTRODUCTION

The growth of rare earth (RE) silicides upon silicon surfaces is of both technological and fundamental interest due to the identification of possible device applications and the unusual reconstructions formed.[1] These unique structures and the discovery of unusually low Schottky barrier heights (0.3–0.4 eV) when formed on *n*-type silicon[2,3] have motivated further characterization of such systems. Subsequently, many studies of different REs on the clean surfaces of Si(100) and Si(111) have been reported in the literature. The RE silicides display a good lattice match to Si(111) substrates which has motivated many studies of the two-dimensional (2D) and three-dimensional (3D) silicides grown on this surface.[4–26]

The 2D silicides are reconstructions which consist of a single monolayer of RE in T4 sites on a Si(111) substrate.[5–16] Above this layer sits a buckled bilayer of silicon, which has its buckling orientation reversed relative to that of the substrate (*B*-type). Extending this structure over several layers results in the 3D RE silicide. These are very similar to the bulk RE silicides with alternating flat layers of RE and Si strained to fit the Si(111) surface unit cell. Figure 1 shows a schematic of this reconstruction, with one of the many configurations of vacancies shown, as determined by Lohmeier *et al.*[17] The presence of these ordered vacancies in the flat Si layers generates a $(\sqrt{3} \times \sqrt{3})R30°$ low-energy electron diffraction (LEED) pattern. This one in six missing Si atoms results in the $RESi_{1.7}$ stoichiometry and is present to relieve the strain induced by the flattening of the Si layers.

It has been established through a variety of different techniques that the surface of the 3D silicide possesses a buckled bilayer similar to that of the 2D silicide.[18–26] However a quantitative analysis of the structure has not been possible until recently. The surface x-ray diffraction (SXRD) study of Lohmeier *et al.*[17] was able to observe subtle effects occurring in the "bulk" of this reconstruction, such as the vacancy induced lateral shifts of Er and Si atoms, but they were unable to determine the structure of the surface due to the large mass contrast between Er and Si and the small occupancy of the surface layer. Thus they assumed the reverse buckled bilayer of the 2D silicide. This assumption has seemingly been confirmed by a variety of techniques such as ARUPS,[18,19] STM,[20–24] and DFT.[26]

STM studies provide evidence of a buckled bilayer of Si which displays $\sqrt{3}$ modulations.[20–24] However, the exact nature of these modulations is not resolved. Roge *et al.*[20] and Wetzel *et al.*[21] observed additional buckling within the Si1 layer (labeling as in Fig. 1) which was attributed to vertical relaxations of surface atoms due to the ordered vacancy network below. Martín-Gago *et al.*[22,23] also observed vacancy induced relaxations at the surface, but they interpreted these as lateral shifts of the Si1 atoms due to vacancies below the Si2 atoms, resulting in "trimers" at the surface. However, a recent theoretical study has interpreted the observed STM contrast $(\sqrt{3} \times \sqrt{3})R30°$ modulations as spectroscopic effects induced by the underlying vacancy network.[27]

The first study able to exclusively determine the structure of the surface bilayer on a 3D RE silicide was a recent LEED study of a thick Y silicide on Si(111) by Rogero *et al.*[25] This LEED analysis is quite complex since deeper surface layers need to be considered along with nonstructural parameters to fully optimise this surface. They concluded that there was a buckled bilayer with significantly enhanced vibrations present at the surface. Further interest comes from the fact that Y silicide has a near perfect lattice match to the Si(111) surface which greatly reduces the effect of strain on the surface structure. Based on the interpretation of strain in the 2D RE silicides by Bonet *et al.*,[13] it is expected that the strain induced for the case of Ho would reduce the *c*-axis lattice spacings due to the expanded *a*-axis resulting from the −0.63% lattice mismatch with the Si(111) surface unit cell. This difference in strain makes a comparison between thick Ho and Y silicides on the Si(111) surface interesting, both in

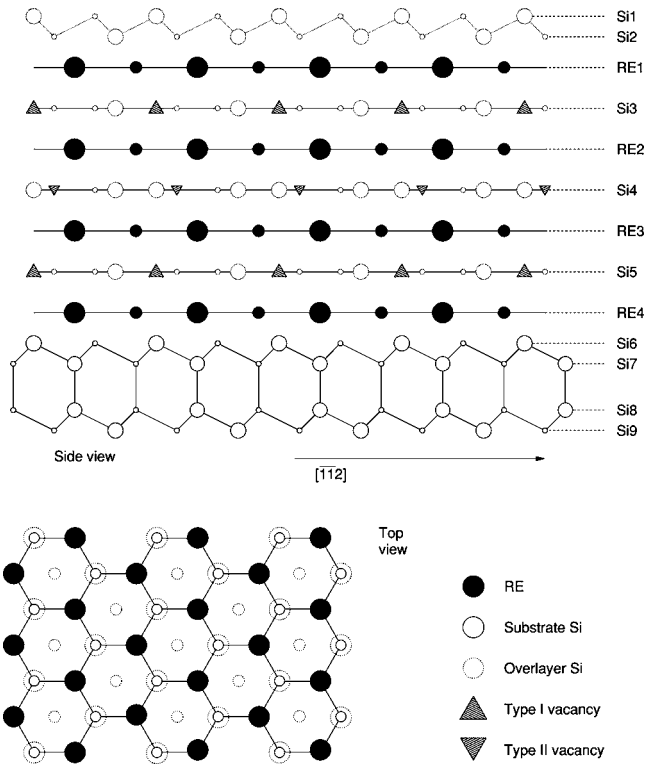

FIG. 1. The structural model for the 3D RE silicides as proposed by Lohmeier *et al.*[17]

terms of the *c*-axis and the detailed surface termination.

Double alignment medium-energy ion scattering (MEIS) has been widely used to study the RE silicides on Si.[11–14] It is particularly powerful for studying the present class of system due to the large mass separation of Ho and Si. The physics of the scattering process allow the scattering yield from each element to be analyzed independently.[28] This proves particularly useful for the 2D RE silicides since any blocking features in the RE signal will be due to the surface bilayer. Thus in MEIS studies of the 2D silicides, only two structural parameters require optimization where other techniques, such as LEED, require the substrate relaxations to be taken into account. In the case of the 3D silicides, MEIS proves particularly powerful since it is possible to align in a variety of geometries which focus on particular aspects of the surface structure. A structural solution for the surface bilayer, which is completely independent of the subsurface structure is possible since aligning along normal incidence illuminates the top Ho layer only, simplifying the problem to a 2D silicide-like optimization.

What follows is an outline of the experimental procedure used to prepare and characterize the surface of 3D Ho silicides. A detailed analysis is then discussed which breaks this complex system down into a series of small experiments which can reveal different aspects of the surface and subsurface structure, allowing a full solution to be determined.

II. EXPERIMENT

All experiments were conducted under ultrahigh vacuum (UHV), with typical base pressures of 2×10^{-10} mbar. Clean

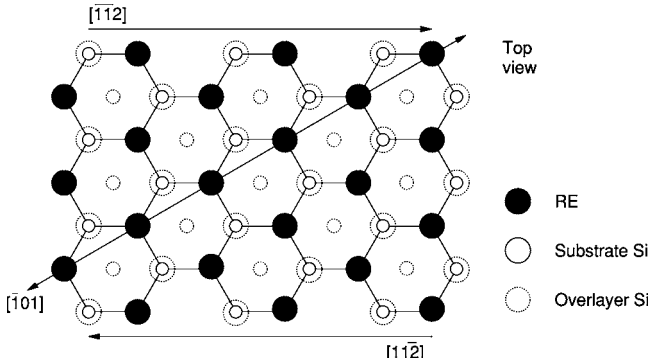

FIG. 2. A top down view of the three azimuths used in this study.

Si(111) samples (cut from a lightly doped *n*-type wafer) were prepared by *e*-beam heating to ~1200 °C for 1 min, then slowly cooled (<100 °C min^{-1}) between 1000 °C and 600 °C to ensure an ordered surface was obtained. Temperature measurements were made using an infrared pyrometer. The heating cycles were repeated until a sharp 7×7 LEED pattern was observed.

The 3D silicide was prepared by depositing approximately 6 ML (relative to the Si(111) surface unit cell) of Ho from a tantalum boat onto the clean Si(111) surface, which was held at ~500 °C during deposition and for 5 min afterwards. The pressure was not allowed to rise above 1×10^{-9} mbar during evaporation and the coverage was determined using a quartz crystal microbalance and the MEIS energy spectrum. When a sharp $(\sqrt{3}\times\sqrt{3})R30°$ LEED pattern was observed the sample was transferred under UHV into the ion scattering chamber.

All MEIS data were acquired at the UK MEIS Facility, CCLRC Daresbury Laboratory, which has been described in detail elsewhere.[29] The ion scattering was conducted using 100 keV H^+ and 50 keV He^+ ions in a variety of geometries. The combination of both H^+ and He^+ were chosen since the surface sensitivity of these beam types differs.[28,30] The greater surface sensitivity of He^+ allows the elucidation of the structure of the top few layers, whereas H^+ reveals the structure of deeper layers. In total five different geometries were used, with each geometry sensitive to different aspects of the 3D silicide structure. To gain sensitivity to the Ho atomic positions, without any blocking contributions from Si atoms, the $[\bar{1}0\bar{2}]/[13\bar{1}]$ geometry was used (incidence/detection directions). This geometry is along the $[\bar{1}01]$ azimuth, and is illustrated in Fig. 2. The other geometries used were $[\bar{1}00]/[110]$, $[0\bar{1}\bar{1}]/[100]$, and the corresponding normal incidence geometries for these two detection directions ($[n]/[110]$ and $[n]/[100]$). These geometries lie along the $[\bar{1}\bar{1}2]$ and $[11\bar{2}]$ azimuths and have been used extensively in previous studies of two-dimensional rare earth silicides since they reveal the positions of the Si bilayer atoms in the reconstruction.[11–14,31]

The MEIS spectra confirmed that the samples were free of contaminants (e.g., O and C) as the only surface peaks observed were Ho and Si. Data were acquired with a beam size of 0.5 mm vertical and 1.0 mm horizontal for a total dose of

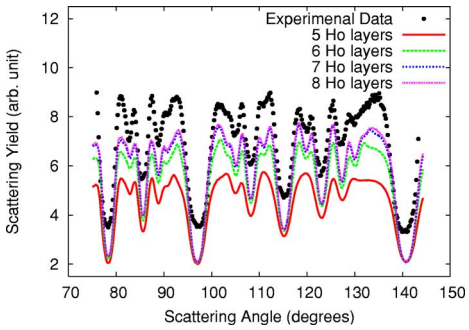

FIG. 3. (Color online) The effect of varying the number of layers in the $[\bar{1}0\bar{2}]/[13\bar{1}]$ geometry. Simulations of 5–8 layers are shown with the experimental data offset for clarity.

$\sim 10^{16}$ ions cm^{-2}. This beam dose is sufficient to allow good statistics, while minimizing the level of beam-induced damage.[11–14,31]

Analysis of MEIS data was accomplished through comparison of experimental data to Monte Carlo simulations of postulated models. The simulations were done using XVegas, a multiplatform version of the Vegas code originally developed by the FOM institute.[32,33] The optimization and comparison to experimental data was achieved using the chi-squared R factor, R_χ.[34,35]

III. RESULTS AND DISCUSSION

A. Determining the number of Ho layers using 100 keV H^+ ions

Before any full analysis of the structure could be conducted the number of layers of Ho contributing to the blocking curves was determined. This was most straightforwardly performed using the scattered ion yield from the Ho atoms in the $[\bar{1}0\bar{2}]/[13\bar{1}]$ geometry, which only displays blocking features due to Ho atoms. The alternative approach of using an absolute yield calibration would not yield this information. This is due to the surface roughness of the RE silicides, which would mean that the number of MLs of RE determined by absolute calibration would not necessarily correspond to the number of layers in the reconstruction—the number of blocking features yields this information directly, provided the ion beam penetrates to the interface.

Figure 3 shows the experimental data fitted to simulations of 5–8 layers of Ho, with the Ho-Ho separation set to 4.01 Å for all layers (which is the best-fit layer spacing for this geometry). There are negligible differences in the blocking curves for 7 layers and over due to shadowing eliminating any yield from subsequent layers. For fewer than 7 layers, the subtle features present in the experimental data are not reproduced, with the main difference between 6 and 7 layers being the rounding off at the top of the feature at 135°. Hence by carefully fitting subtle features in the data it has been determined that at least seven layers must be contributing to these blocking curves. This is consistent with the surface roughness observed for the RE silicides whereby islands of differing heights grow after an initial layer is formed. This would explain how a 6 ML deposit displays features due to extra layers since the 7 layer structure will start to form before the 5 and 6 layer film is complete. Hence a mixture of different thicknesses of this reconstruction may be observed.

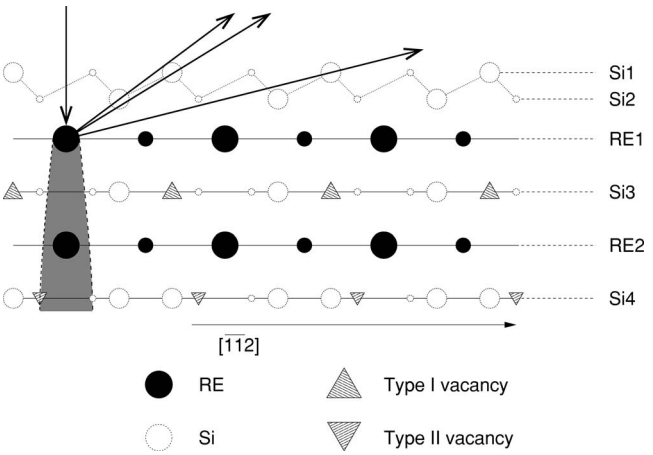

FIG. 4. Normal incidence geometries eliminate contributions from lower Ho layers due to the effects of shadowing if a 50 keV He^+ beam is used. Hence features due to the surface bilayer alone make up the blocking curves for such geometries.

B. The surface bilayer: 50 keV He^+ scattering

Figure 4 shows the type of geometry that was used to obtain structural information about the surface bilayer. Aligning a 50 keV He^+ beam normal to the surface, it was possible to illuminate just the top layer of Ho, since all other RE atoms lie inside its shadow cone (the shadow cone radius for the conventional 100 keV H^+ beam is too small, such that there is significant illumination of the second Ho layer which complicates the fitting process[36]). Since He^+ is more damaging to the surface than H^+, low beam doses were used to study a large area of the sample. This allowed an exclusive determination of the structure of the surface bilayer.

In total six samples were prepared under nominally the same conditions and exposed to the 50 keV He^+ beam. Five of these samples displayed a sixfold symmetric LEED pattern and almost identical blocking curves, and were taken to be representative of a typical termination of the 3D Ho silicide. Data from these five samples were summed to give the blocking curves shown in Fig. 5(a). It is clear that the observed sixfold symmetry in the LEED pattern is replicated in these blocking curves as they show a high level of symmetry for geometries along opposing azimuths. These blocking curves are the result of a mixture of a B-type Si bilayer as observed on the 2D RE silicides,[5–15] and an A-type termination which has previously only been observed for 2D silicides after exposure to atomic hydrogen.[31] Figure 5(b) shows which atoms cause each of the observed features.

This observation of differing buckling orientations is probably due to the presence of the vacancy network in this class of system. There is much contention in the literature regarding the ordering of the underlying vacancy network, with periodicities of $1c$, $2c$, and $3c$ all being reported.[17,37–42] The observation of a particular buckling orientation could be linked to the presence of a particular vacancy type in the

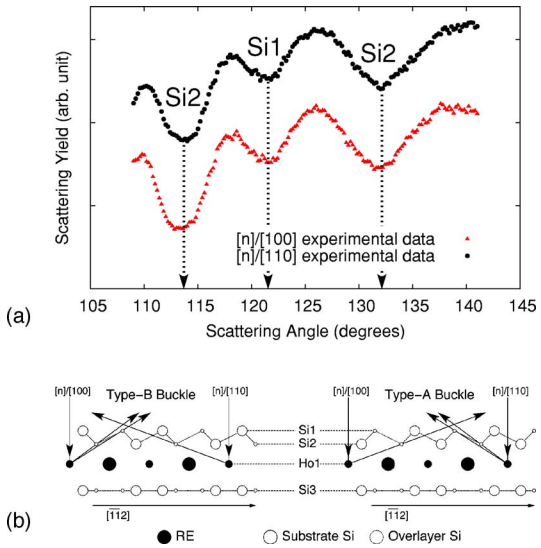

FIG. 5. (Color online) (a) The symmetrical MEIS blocking curves obtained by summing data sets from the five samples which displayed sixfold symmetry in the LEED pattern. Data were acquired using 50 keV He^+ ions. The blocking curves are offset along the *y*-axis for clarity. (b) A side view schematic showing which atoms cause each of the observed features.

top-most flat Si layer (Si3). Recent STM studies have suggested that the topmost vacancy always lies beneath the Si2 atoms.[22,23,43] If this is true then two differing interpretations can be applied to the A/B mixed phase. If the vacancy network is well ordered throughout the silicide, the surface roughness would result in differing thicknesses of silicide displaying different terminations if the periodicity is $2c$ or $3c$ (to maintain the vacancy being below the Si2 atom). This assumes that the vacancy position is fixed at the interface. The alternative to this is that the ordering of the vacancy network is only present in the top few layers, with the ordering at the interface being poor. If this were the case then, there would be nothing to "fix" the order of the vacancies so the resulting structure will display a mixture of *A*- and *B*-type terminations. In this model the number of layers has no effect on the buckling orientation.

The sixth sample that was analyzed using a 50 keV He^+ beam is quite different to the typical A/B termination reported above. The blocking curves for this sample are shown in Fig. 6. This sample displayed threefold symmetry which is due to the almost complete absence of the blocking features associated with the *B*-type termination and the dominance of

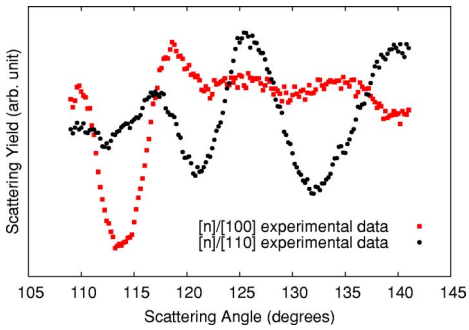

FIG. 6. (Color online) 50 keV He^+ MEIS blocking curves from the surface displaying threefold symmetry, which are typical of an *A*-type Si bilayer termination.

blocking dips associated with the *A*-type termination. MEIS is able to resolve the difference between an *A*- and *B*-type bilayer since by aligning along a known bulk Si direction, the blocking features observed give the buckling orientation [see Fig. 5(b)]. It is interesting to note that at no point has a sample been prepared that exclusively displays the *B*-type termination observed for 2D RE silicides, and which has been assumed in previous work on 3D RE silicides.[17,20–25] This is the first time a predominantly *A*-type termination has been directly observed on this class of system. The existence of such a phase demonstrates that under very specific conditions the surface shows a preference for a particular orientation of the Si bilayer. This preference for an *A*-type termination could be due to either a $1c$ ordering of the vacancies along the *c*-axis, or the presence of a particularly flat 6 ML reconstruction, with very little islanding and the vacancy order fixed at the interface. The latter seems unlikely due to the known surface roughness of the RE silicides. A recent LEED and STM study of Y silicide has demonstrated this variability in height over the length scale which is observed in MEIS.[44]

1. The A/B mixed phase

Before a final structural solution can be determined, it is necessary to ensure that the blocking features determined by the simulations are the correct size so that R_χ can select the best-fit structural model.[14,15] One way of doing this is through an evaluation of the nonstructural parameters in this system, i.e., the r.m.s. thermal vibrations of the surface atoms. For the work that follows, it is assumed that the vibrations are isotropic and for the Ho atoms take the bulk metal values of 0.13 Å. This is consistent with the work on the 2D Y silicide which found that it is just the Si bilayer atoms

TABLE I. Optimal surface bilayer r.m.s. thermal vibrations, σ, as determined by R_χ. Values determined for the 3D and 2D Y silicide are given for comparison. The bulk value for Si is 0.075 Å.

Parameter	Si(111)$(\sqrt{3}\times\sqrt{3})R30°$-Ho from this work σ/Å	Si(111)$(\sqrt{3}\times\sqrt{3})R30°$-Y from Ref. 25 (LEED) σ/Å	Si(111)$p(1\times1)$-Y from Ref. 14 (MEIS) σ/Å
σ(Si1)	0.23±0.03	0.22	0.15±0.02
σ(Si2)	0.14±0.01	0.16	0.12±0.02
σ(RE)	0.13 (Fixed)	0.06	0.08

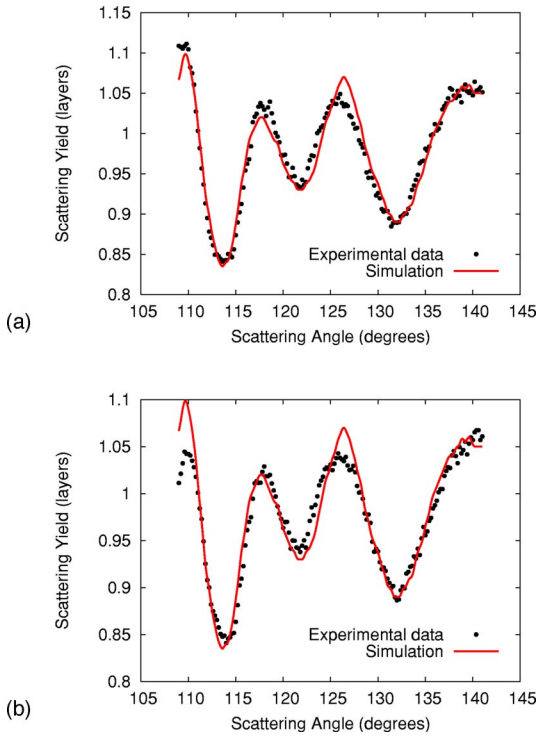

FIG. 7. (Color online) The fits obtained by R_χ for a 50 keV He^+ beam, using the vibrations listed in Table I. The structural parameters are summarized in Table II. (a) The $[n]/[100]$ geometry. (b) The $[n]/[110]$ geometry.

which display a significant vibrational enhancement.[14,15] For a structural model that gave best visual agreement, simulations varying the magnitude of the Si1 and Si2 vibrations were conducted. A χ^2 fitting of these parameters gives the optimal vibrations shown in Table I.

The magnitude of the vibrations determined are significantly enhanced, even more so than the values reported for the 2D silicides.[14,15] Inclusion of such high vibrations in the model is critical if a good structural fit is to be obtained using R_χ, which can be misled by any large discrepancies in the overall fit.[13,14] A further discussion of these vibrational amplitudes in the context of the present system follows the structural optimization.

Initial investigations into the structural parameters of this system revealed that it is not possible to detect differences in the structural parameters of the surface bilayers in *A*-type domains compared with *B*-type domains. Thus in the following analysis, the *A*- and *B*-type terminations are assumed to have the same structural parameters and hence just two parameters require optimization—the Si1-Ho1 layer spacing $z_{\text{Si1-Ho1}}$, and the Si2-Ho1 layer spacing $z_{\text{Si2-Ho1}}$ (which in turn gives the buckling separation $z_{\text{Si1-Si2}}$). Such an optimization yields the fits shown in Fig. 7, with the structural parameters summarized in Table II.

Looking at the size of these parameters, a trend between the bulk silicide interlayer spacing and the 2D and 3D silicide values seems apparent. For the bulk silicide, the distance from the flat Ho layer to the flat Si layer is 2.054 Å.[4] This represents the layer spacing for this system when it is not confined by the requirements of lattice matching to the Si(111) surface. As discussed by Bonet *et al.*,[13] strain will be the driving force for any relaxation observed in the *c*-axis lattice parameters. The 3D Ho silicide grown on Si(111) will represent an intermediate between the 2D silicide and the bulk 3D silicide due to the extra layers present in the growth. Thus the values of the Si2-Ho1 spacing lie between the bulk value of 2.054 Å and the 2D Ho silicide which has a compressed value of 1.86 Å. The observed bilayer rumpling of the 3D silicide is reduced when compared to the 2D silicide, which again could be due to the relief of strain in the surface, through the presence of vacancies in the lower flat Si layers. These observations are consistent with the results of the LEED study of 3D Y silicide on Si(111).[25]

2. Beam induced damage

The 50 keV He^+ beam that is used to gain maximum surface sensitivity in this study will broaden the observed blocking features due to the effects of damage and disorder. These have been accounted for by allowing R_χ to choose significantly enhanced vibrations. Care was taken when collecting the data to minimize damage effects, but prevention was not possible. Figure 8 demonstrates how the blocking curves change when a single sample point is exposed to a series of 1.5 μC He^+ doses. It appears that under exposure to a 50 keV He^+ beam, the Si1 layer is either removed or amorphized quite rapidly while the level of damage accumulated in the Si2 layer is small in comparison. The rate of damage to the Si1 layer is such that after a 3.0 μC dose, the Si1 feature has almost disappeared. The Si2 damage appears to accumulate more slowly as the two Si2 features in the data persist, even after a high beam dose. With this in mind, it has been possible to form a simple model for how the damage accumulates at the surface based on the combination of simulations of differing states of damage at the surface (see the Appendix).

TABLE II. Optimal surface bilayer layer spacings for Si(111)$(\sqrt{3}\times\sqrt{3})R30°$-Ho using MEIS as obtained using R_χ. Values for the 2D Ho silicide and 3D Y silicide are given for comparison.

Parameter	Si(111)$(\sqrt{3}\times\sqrt{3})R30°$-Ho from this work z/Å	Si(111)(1×1)-Ho from Ref. 13 (MEIS) z/Å	Si(111)$(\sqrt{3}\times\sqrt{3})R30°$-Y from Ref. 25 (LEED) z/Å
$z_{\text{Si1-Ho1}}$	2.75±0.03	2.69±0.02	2.69±0.06
$z_{\text{Si2-Ho1}}$	1.96±0.01	1.86±0.02	2.01
$z_{\text{Si1-Si2}}$	0.79±0.03	0.83±0.03	0.68

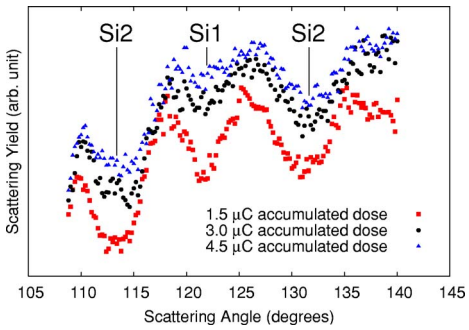

FIG. 8. (Color online) The results of an experimental damage survey in the $[n]/[100]$ geometry. The same sample point was exposed to a series of 1.5 μC He^+ doses. The Si1 blocking features accumulate damage more rapidly than the Si2 features.

This simple model allows the reevaluation of the structural model for the 3D Ho silicide using lower r.m.s. thermal vibrations, indicating that some of the enhanced vibrations may be due to static disorder and damage. A precise determination of the magnitude of the surface vibrations is not possible at present, as it would be necessary to conduct low temperature experiments to be able to separate out the effects of damage, static disorder, and thermal vibrations. Thus for the following model, He^+ damage has been modeled explicitly allowing a reduced enhancement of the thermal vibrations. The surface bilayer vibrations are set to those determined in a recent MEIS study of the 2D Y silicide surface.[14] The 2D Y silicide system displays enhanced vibrations which seem more physically reasonable than the values determined by R_χ in the present work (see Table I). Incorporating this model into the simulations used to fit the high quality data sets with good statistics, allowed a full structural optimization to be conducted which resulted in the fits shown in Fig. 9 and the associated parameters in Table III.

As can be seen in Fig. 9, the agreement between experiment and simulation is excellent, even though the r.m.s. thermal vibrations of the top bilayer have been greatly reduced (0.08 Å lower in the case of Si1 atoms, see Table I) and a simple model of damage and disorder has been applied. While no quantitative analysis of the surface vibrations is possible with the current data, a qualitative comparison of the fits in Figs. 7 and 9 suggests that the fits obtained by damage modeling are an improvement over those for enhanced vibrations. For example the damage modeling does not overbroaden the Si1 features as is the case for significantly enhanced vibrations. These lower vibrational amplitudes also seem more physically reasonable when compared to the enhanced values determined in the absence of damage modeling.

The structural parameters determined for both enhanced vibrations and damage modeling show an excellent level of agreement as they are the same within the limit of the errors. This demonstrates how MEIS is able to separate the effects of structural and nonstructural parameters on the blocking curves obtained, allowing determination of the interlayer spacings in such a reconstruction even though the exact values of the r.m.s. thermal vibrations are not known. Such factors can complicate other surface crystallography techniques such as quantitative LEED.

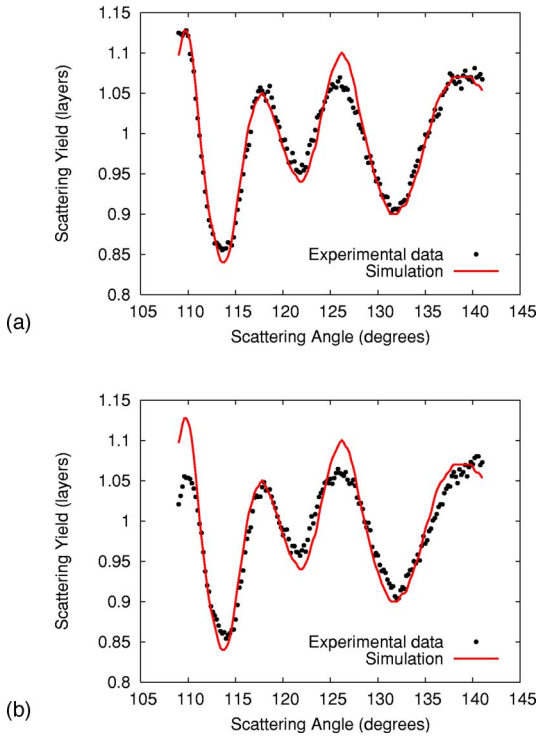

FIG. 9. (Color online) The fits obtained by R_χ using 50 keV He^+ and a simple model of damage evolution. The structural parameters are summarized in Table III. (a) The $[n]/[100]$ geometry. (b) The $[n]/[110]$ geometry.

This observed mixture of both *A*- and *B*-type buckled bilayers is not surprising since it is expected that the *B*-type bilayer of the 2D RE silicides is the result of the interaction between the substrate and surface layers. For the 3D silicides, the greater thickness of the film reduces such effects. It is proposed that the underlying vacancy network will control the buckling orientation of the surface. The observation of a mixture of both orientations and the contention present in the literature regarding the ordering of these vacancies,[17,37–42] suggests that the vacancy network is either disordered at the interface or that the surface roughness causes domains with differing numbers of layers to have different terminations, under these preparation conditions. However, the observation of a threefold symmetric surface under certain conditions suggests that it is possible to create very specific 1*c* ordering within this network, resulting in a predominantly *A*-type termination.

TABLE III. Optimal surface bilayer layer spacings for Si(111) $(\sqrt{3}\times\sqrt{3})R30°$-Ho where He^+ damage has been modeled explicitly instead of using enhanced vibrations.

Parameter	Damage modeling z/Å	Enhanced vibrations z/Å
$z_{\text{Si1-Ho1}}$	2.76±0.04	2.75±0.03
$z_{\text{Si2-Ho1}}$	1.97±0.01	1.96±0.01
$z_{\text{Si1-Si2}}$	0.79±0.04	0.79±0.03

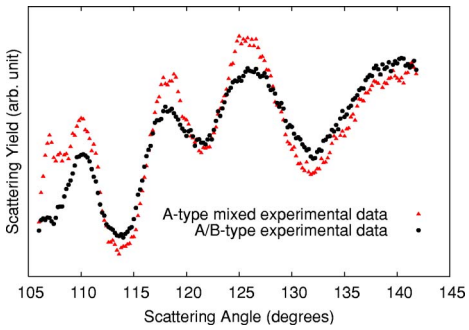

FIG. 10. (Color online) A comparison of 50 keV He^+ data from the A/B mixed phase and the predominantly A-type terminated surface. The A-type data from both geometries have been summed to restore the sixfold symmetry in the MEIS data and allow a comparison with the data from the A/B mixed phase. The resulting curves look very similar to the A/B mixed phase.

3. The A-type termination

To enable a comparison of the threefold A-type data to the mixed A/B phase, it is possible to sum the scattering yield from two 180° rotated geometries to create a sixfold symmetric blocking curve. This allows a direct comparison of the positions of the blocking features caused by the A-type domains in both structures. Figure 10 demonstrates how similar the blocking curves are for the A/B mixed phase and the symmetrized predominantly A-type structure. They show a high level of agreement, suggesting that the structures of the A-type domains in these two phases are very similar. To further emphasize this point, a fitting of the experimental data from the threefold A-type terminated surface is possible, with the fits shown in Fig. 11 and the lattice spacings summarized in Table IV.

These fits were obtained by using the damage model proposed in the previous section, and fitting $z_{\mathrm{Si1\text{-}Ho1}}$ and $z_{\mathrm{Si2\text{-}Ho1}}$. It was established that by using the alternative procedure of applying enhanced vibrations, a slightly poorer fit was obtained in the flat regions of these data sets, due to the illumination of deeper layers of the reconstruction. A 10% mixture of B-type Si bilayer was also used, since a subtle visual improvement in the fit was obtained.

The parameters determined in Table IV demonstrate the observed similarity in the blocking curves for all data sets obtained, as the lattice spacings for the two phases agree within the limits of the errors.

C. The full structure

Having established the true nature of the surface bilayer, it was possible to fit further 100 keV H^+ data in the $[\bar{1}00]/[110]$, $[0\bar{1}\bar{1}]/[100]$, and $[\bar{1}0\bar{2}]/[13\bar{1}]$ geometries to gain an insight into the structure of deeper surface layers. Using such geometries it was possible to determine the layer spacing between subsequent Ho layers. However, these geometries are not sensitive to the position of the flat Si layers in this reconstruction as the curves are dominated by Ho-Ho blocking features due to Ho being a much stronger scatterer than Si. As a result of this, it is assumed that the Si

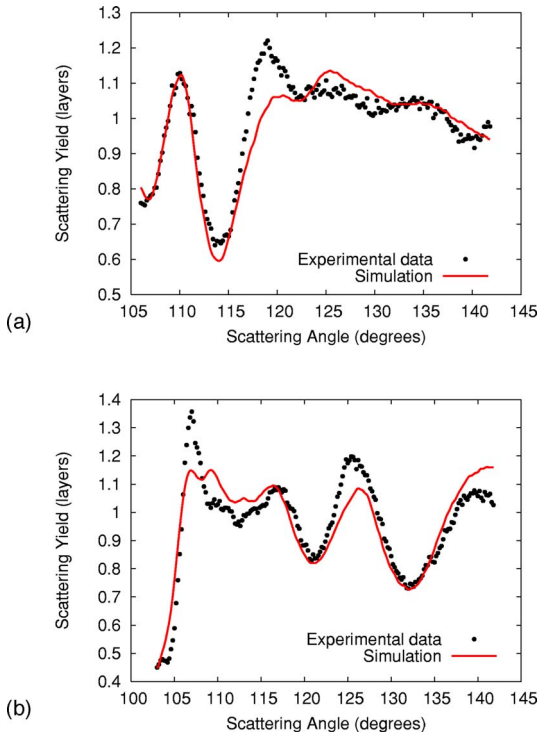

FIG. 11. (Color online) The fits obtained for the A-type termination by R_χ using 50 keV He^+ and a simple model of damage evolution. The structural parameters are summarized in Table IV. (a) The $[n]/[100]$ geometry. (b) The $[n]/[110]$ geometry.

layers lie exactly in the middle of the Ho layers, due to the symmetry of such a structure. It is also assumed that we are observing the typical A/B mixed phase which occurs most readily and is characterized by the sixfold symmetric LEED pattern. The lattice spacings of the surface bilayer have been set to the values determined using the damage model in the analysis described in Sec. III B.

The r.m.s. thermal vibrations of the Ho and flat layer Si atoms in this reconstruction were set to enhanced values of 0.15 Å and 0.13 Å respectively, for these geometries. These values were determined in preliminary simulations which demonstrated that the presence of vacancies, and the resulting lateral shifts of neighboring atoms, have the same affect on the blocking curves as enhanced vibrations. The fits determined are shown in Fig. 12 with a full summary of the parameters determined in this study shown in Table V.

The 100 keV H^+ data reveals that the Ho-Ho interlayer spacing is compressed relative to that of the bulk silicide,

TABLE IV. Optimal surface bilayer layer spacings for a predominantly A-type termination of $Si(111)(\sqrt{3}\times\sqrt{3})R30°$-Ho where He^+ damage has been modeled.

Parameter	A-type termination z/Å	A/B mixed phase z/Å
$z_{\mathrm{Si1\text{-}Ho1}}$	2.70±0.05	2.76±0.03
$z_{\mathrm{Si2\text{-}Ho1}}$	2.00±0.02	1.97±0.01
$z_{\mathrm{Si1\text{-}Si2}}$	0.70±0.05	0.79±0.03

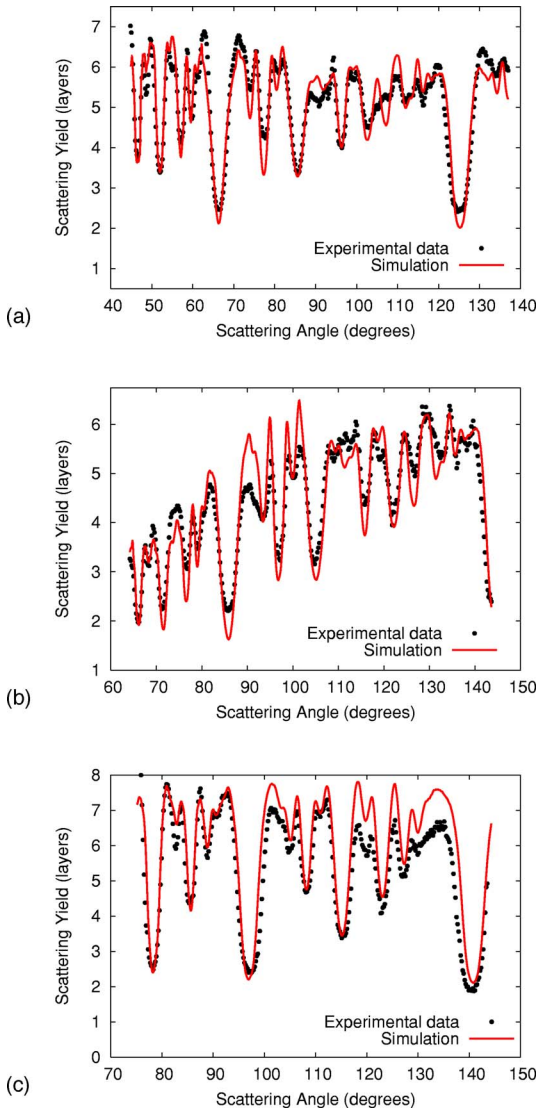

FIG. 12. (Color online) The fits obtained using 100 keV H^+ in a variety of geometries. The structural parameters are summarized in Table V. (a) The $[\bar{1}00]/[110]$ geometry, (b) the $[0\bar{1}\bar{1}]/[100]$ geometry, and (c) the $[\bar{1}0\bar{2}]/[13\bar{1}]$ geometry.

taking values of 4.01±0.02 Å and 4.108 Å (Ref. 4), respectively. This is expected since the strain induced by the lattice match to the Si(111) surface requires the *a*-axis of the silicide to be expanded for the requirements of epitaxy. Hence this result is consistent with the study by Bonet *et al.*,[13] who demonstrated that such strain is compensated by a relaxation of the *c*-axis lattice spacing in the case of the 2D RE silicides.

TABLE V. The optimal surface layer spacings for Si(111)$(\sqrt{3}\times\sqrt{3})R30°$-Ho. The Si bilayer spacings are set according to Table III and the flat Si layers were confined to lie in the middle of the two adjacent Ho layers. The r.m.s thermal vibrations were set to the values used in the damage model.

Parameter/Å	
$z_{\text{Si1-Ho1}}$	2.76±0.03
$z_{\text{Si2-Ho1}}$	1.97±0.01
$z_{\text{Si1-Si2}}$	0.79±0.03
$z_{\text{Ho-Ho}}$	4.01±0.02
$z_{\text{Ho-Si}}$	2.005
σ(Si1)	0.15
σ(Si2)	0.12
σ(RE)	0.13

IV. SUMMARY AND CONCLUSIONS

The surface crystallography of 3D Ho silicide grown on the Si(111) surface has been determined using MEIS. A variety of geometries and ion species have been used to extract the maximum amount of structural information from this system. Aligning a 50 keV He^+ beam normal to the surface illuminates the top Ho layer only, allowing the scattered ion yield from the Ho atoms to be used to determine the structure of the surface bilayer. It has been established that the 3D Ho silicide displays two subtly different surface terminations.

The typical termination observed for this system is a mixture of both *A*- and *B*-type Si bilayers. This is characterized by sixfold symmetry in the LEED pattern and MEIS blocking curves. A careful analysis, whereby damage is modeled through the use of enhanced vibrations or a linear damage model, revealed that the structure of both the *A*- and *B*-type terminations are the same. The Si bilayer was found to be sitting 1.97±0.01 Å above the first Ho layer ($z_{\text{Si2-Ho1}}$), with a vertical buckling separation, $z_{\text{Si1-Si2}}$, of 0.79±0.04 Å. It was proposed that the presence of such a mixed orientation phase

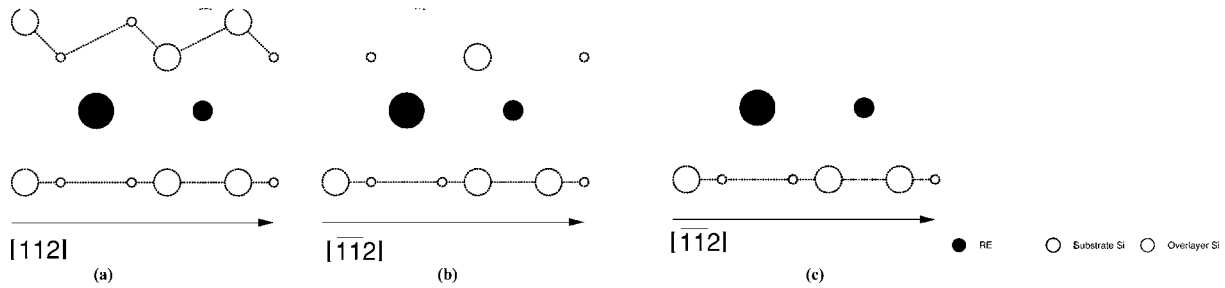

FIG. 13. Side views of the three different structures used to model damage, which are mixed in the ratio *a*:*b*:*c*. (a) A perfect, undamaged surface bilayer, (b) a surface layer which has had the Si1 atoms removed, and (c) a fully damaged surface.

at the surface is due to either a combination of the surface roughness and $2c$ periodicity of the vacancies throughout the crystal, or disorder in the vacancy network at the interface.

The alternative termination is a threefold symmetric A-type bilayer, which displays similar interlayer spacings to the mixed phase. In this case the Si bilayer was found to be 2.00 ± 0.02 Å above the topmost Ho layer, with a buckling separation of 0.70 ± 0.06 Å. These values agree within error with the values obtained for the A/B phase. This preference for the A-type termination may be due to $1c$ ordering of the vacancy network below.

Both these terminations are present on top of the established layered structure of the 3D silicide. Using 100 keV H^+ in a variety of geometries, it has been established that there are at least seven layers in this reconstruction with a Ho-Ho vertical spacing of 4.01 ± 0.02 Å. This layer spacing is compressed relative to the bulk silicide value, which can be explained by the relief of strain induced due to lattice matching.

ACKNOWLEDGMENTS

The authors would like to acknowledge the Engineering and Physical Science Research Council for funding this research. Paul Quinn and the FOM institute are thanked for supplying the XVegas and Vegas simulation codes. The assistance and technical support of Kevin Connell and Mark Pendleton are also much appreciated.

APPENDIX: DAMAGE MODELING

To model the accumulation of damage at the surface, a variety of simulations have been combined to produce a "damaged" surface using XVegas. First, a simulation of a perfect surface was performed where the Si1 and Si2 atomic positions were varied. This represents the ideal situation of no damage accumulation in the surface layers. A second simulation where the Si1 layer is removed from the surface and the Si2 atomic positions are varied represents a surface which has been subjected to Si1 damage. Finally a simulation whereby the surface bilayer is removed from the surface produces an almost flat blocking curve (with subtle modulations due to subsurface illumination). This represents the surface when the bilayer has been completely removed or amorphized, leaving a Ho terminated reconstruction. By then combining these three simulations in a variety of ratios, it was possible to model the damage occurring at the surface (Fig. 13 shows schematics of the different models used). Such ratios take the form $a:b:c$ where a, b, and c represent the percentage of the surface that is not damaged, has the Si1 layer removed, and, has suffered complete removal of the surface bilayer, respectively.

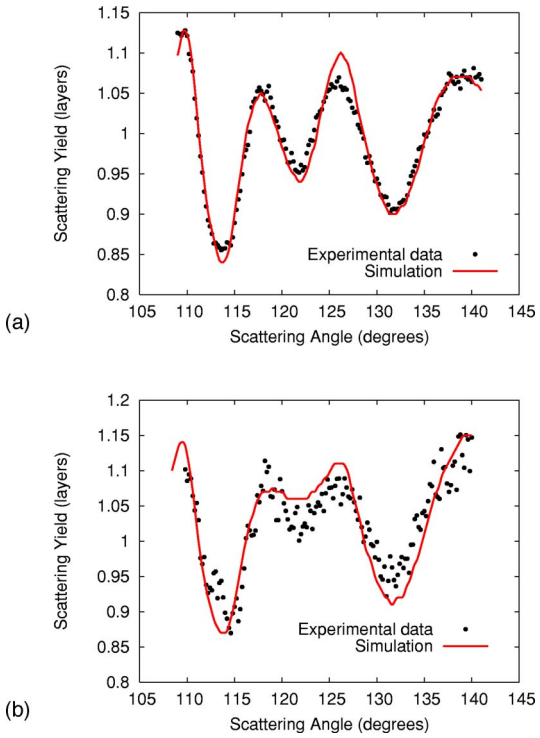

FIG. 14. (Color online) (a) The 1.5 μC experimental data fitted to simulations with a damage ratio, $a:b:c$, of 50:35:15. (b) The 3.0 μC experimental data fitted to simulations with a damage ratio, $a:b:c$, of 0:70:30. Both fits are for 50 keV He^+ in the $[n]/[100]$ geometry.

To determine the ratio of the three simulations, it has been assumed that damage accumulation is linear. A fitting of the 1.5 μC data was conducted for a variety of ratios, then a similar fitting was conducted for the 3.0 μC data but with double the damage ratios that appeared suitable for the lower dose. The damage ratio that fitted both data sets was chosen as representing the "correct" model for damage evolution. This ratio was determined by assessing which model gave the best visual agreement, since the main aim of this work is to show how damage *could* explain the high vibrations observed. The ratio that was found to work best after a 1.5 μC dose was 50:35:15 and hence 0:70:30 for the 3.0 μC data. The fits are shown in Fig. 14. The experimental data shown in Fig. 14(b) have much poorer statistics compared to those in Fig. 14(a) since the damage survey was only conducted on one sample (there is a factor of 20 difference in the number of counts between the two data sets).

*Electronic address: spt1@york.ac.uk; URL: http://www-users.york.ac.uk/~phys24/

[1] F. P. Netzer, J. Phys.: Condens. Matter **7**, 991 (1995).
[2] K. N. Tu, R. D. Thompson, and B. Y. Tsaur, Appl. Phys. Lett. **38**, 626 (1981).
[3] H. Norde, J. de Sousa Pires, F. d'Heule, F. Pesavento, S. Petersson, and P. A. Tove, Appl. Phys. Lett. **38**, 865 (1981).
[4] J. A. Knapp and S. T. Picraux, Appl. Phys. Lett. **48**, 466 (1986).

[5] P. Paki, U. Kafader, P. Wetzel, C. Pirri, J. C. Peruchetti, D. Bolmont, and G. Gewinner, Phys. Rev. B **45**, 8490 (1992).
[6] P. Wetzel, C. Pirri, P. Paki, D. Bolmont, and G. Gewinner, Phys. Rev. B **47**, 3677 (1993).
[7] L. Stauffer, A. Mharchi, C. Pirri, P. Wetzel, D. Bolmont, G. Gewinner, and C. Minot, Phys. Rev. B **47**, 10555 (1993).
[8] M. H. Tuilier, P. Wetzel, C. Pirri, D. Bolmont, and G. Gewinner, Phys. Rev. B **50**, 2333 (1994).
[9] H. Kitayama, S. P. Tear, D. J. Spence, and T. Urano, Surf. Sci. **482**, 1481 (2001).
[10] C. Bonet, D. J. Spence, and S. P. Tear, Surf. Sci. **504**, 183 (2002).
[11] D. J. Spence, S. P. Tear, T. C. Q. Noakes, and P. Bailey, Phys. Rev. B **61**, 5707 (2000).
[12] D. J. Spence, T. C. Q. Noakes, P. Bailey, and S. P. Tear, Surf. Sci. **512**, 61 (2002).
[13] C. Bonet, I. M. Scott, D. J. Spence, T. J. Wood, T. C. Q. Noakes, P. Bailey, and S. P. Tear, Phys. Rev. B **72**, 165407 (2005).
[14] T. J. Wood, C. Bonet, T. C. Q. Noakes, P. Bailey, and S. P. Tear, Surf. Sci. **598**, 120 (2005).
[15] C. Rogero, C. Polop, L. Magaud, J. L. Sacedón, P. L. de Andrés, and J. A. Martín-Gago, Phys. Rev. B **66**, 235421 (2002).
[16] M. Lohmeier, W. J. Huisman, G. ter Horst, P. M. Zagwijn, E. Vlieg, C. L. Nicklin, and T. S. Turner, Phys. Rev. B **54**, 2004 (1996).
[17] M. Lohmeier, W. J. Huisman, E. Vlieg, A. Nishiyama, C. L. Nicklin, and T. S. Turner, Surf. Sci. **345**, 247 (1996).
[18] P. Wetzel, S. Saintenoy, C. Pirri, D. Bolmont, and G. Gewinner, Phys. Rev. B **50**, 10886 (1994).
[19] L. Stauffer, A. Mharchi, S. Saintenoy, C. Pirri, P. Wetzel, D. Bolmont, and G. Gewinner, Phys. Rev. B **52**, 11932 (1995).
[20] T. P. Roge, F. Palmino, C. Savall, J. C. Labrune, P. Wetzel, C. Pirri, and G. Gewinner, Phys. Rev. B **51**, 10998 (1995).
[21] P. Wetzel, S. Saintenoy, C. Pirri, D. Bolmont, G. Gewinner, T. P. Roge, F. Palmino, C. Savall, and J. C. Labrune, Surf. Sci. **355**, 13 (1996).
[22] J. A. Martín-Gago, J. M. Gómez-Rodríguez, and J. Y. Veuillen, Surf. Sci. **366**, 491 (1996).
[23] J. A. Martín-Gago, J. M. Gómez-Rodríguez, and J. Y. Veuillen, Phys. Rev. B **55**, 5136 (1997).
[24] C. Polop, C. Rogero, J. L. Sacedón, and J. A. Martín-Gago, Surf. Sci. **482-485**, 1337 (2001).
[25] C. Rogero, P. L. de Andres, and J. A. Martín-Gago, Phys. Rev. B **71**, 165306 (2005).
[26] L. Magaud, A. Pasturel, G. Kresse, and J. Hafner, Phys. Rev. B **58**, 10857 (1998).
[27] E. Duverger, F. Palmino, E. Ehret, and J. C. Labrune, Surf. Sci. **595**, 40 (2005).
[28] J. F. van der Veen, Surf. Sci. Rep. **5**, 199 (1985).
[29] P. Bailey, T. C. Q. Noakes, and D. P. Woodruff, Surf. Sci. **426**, 358 (1999).
[30] I. Stensgaard, Rep. Prog. Phys. **55**, 989 (1992).
[31] D. J. Spence, T. C. Q. Noakes, P. Bailey, and S. P. Tear, Phys. Rev. B **62**, 5016 (2000).
[32] R. M. Tromp and J. F. van der Veen, Surf. Sci. **133**, 159 (1983).
[33] J. W. M. Frenken, J. F. van der Veen, and R. M. Tromp, Nucl. Instrum. Methods **17**, 334 (1986).
[34] T. C. Q. Noakes, P. Bailey, and D. P. Woodruff, Nucl. Instrum. Methods Phys. Res. B **136-138**, 1125 (1998).
[35] D. Brown, T. C. Q. Noakes, D. P. Woodruff, P. Bailey, and Y. le Goaziou, J. Phys.: Condens. Matter **11**, 1889 (1999).
[36] It is actually the interplay of thermal vibrations and the size of the shadow cone which cause this effect. Cooling the sample to reduce thermal vibrations would also greatly reduce the ion yield from deeper layers. This was not possible with the current experimental setup.
[37] L. Magaud, A. Pasturel, G. Kresse, and J. Hafner, Phys. Rev. B **55**, 13479 (1997).
[38] L. Stauffer, C. Pirri, P. Wetzel, A. Mharchi, P. Paki, D. Bolmont, G. Gewinner, and C. Minot, Phys. Rev. B **46**, 13201 (1992).
[39] R. Baptist, S. Ferrer, G. Grenet, and H. C. Poon, Phys. Rev. Lett. **64**, 311 (1990).
[40] C. H. Luo, G. H. Shen, and L. J. Chen, Appl. Surf. Sci. **113/114**, 457 (1997).
[41] T. L. Lee, L. J. Chen, and F. R. Chen, J. Appl. Phys. **71**, 3307 (1992).
[42] K. S. Chi, W. C. Tsai, and L. J. Chen, J. Appl. Phys. **93**, 153 (2003).
[43] I. Engelhardt, C. Preinesberger, S. K. Becker, H. Eisele, and M. Dähne, Surf. Sci. **600**, 755 (2006).
[44] C. Rogero, C. Polop, J. L. Sacedón, and J. A. Martín Gago, Surf. Interface Anal. **36**, 1195 (2004).